# All-optical wavelength shifting in a semiconductor laser using resonant nonlinearities

Julien Madéo, P. Cavalié, Joshua R. Freeman, Nathan Jukam, Jean Maysonnave, Kenneth Maussang, Harvey E. Beere, David A. Ritchie, Carlo Sirtori, Jérôme Tignon, et al.

# All-optical wavelength shifting in a semiconductor laser using resonant nonlinearities

Julien Madéo,[1] Pierrick Cavalié,[1] Joshua R. Freeman,[1] Nathan Jukam,[1] Jean Maysonnave,[1] Kenneth Maussang,[1] Harvey. E. Beere,[2] David. A. Ritchie,[2] Carlo Sirtori,[3] Jérôme Tignon[1] and Sukhdeep S. Dhillon[1]

[1]Laboratoire Pierre Aigrain, Ecole Normale Supérieure, UMR 8551 CNRS, Université P. et M. Curie, Université D. Diderot, 24 rue Lhomond, 75005 Paris, France
[2] Semiconductor Physics Group, University of Cambridge, JJ Thomson Avenue, Cambridge CB3 0HE, UK
[3]Matériaux et Phénomènes Quantiques, Université Denis Diderot - Paris 7, UMR 7162 CNRS, 75013 Paris, France

**For future ultrafast all-optical networks, new optical devices are required that directly manipulate communication channels to shift their wavelength over the bandwidth of an optical fiber (50THz).[1,2] Current proposed solutions based on nonlinear processes, however, suffer from small efficiencies owing to low nonlinear susceptibilities.[3] Here, we demonstrate all-optical wavelength conversion of a near-infrared beam using a resonant non-linear process within a terahertz (THz) quantum-cascade-laser (QCL).[4] The process is based on injecting a low power CW near-infrared beam in resonance with the interband transitions of the QCL. This results in an enhanced nonlinearity allowing the efficient generation of the difference and sum frequency, shifting the frequency of the near-infrared beam by the QCL frequency. Efficiencies of 0.13% are shown which are equivalent to those obtained using Free Electron Lasers. As well as important implications as an ultrafast wavelength shifter, this work also opens up the possibility of efficiently up-converting THz radiation to the near-infrared and the study of high THz-optical field interactions with quantum structures using QCLs.**

Wavelength division multiplexing (WDM) is currently used extensively in optical fibre networks to enhance the carrier capacity of optical fibres where each wavelength in a multi-wavelength bunch is assigned to a particular communication channel.[5] In these types of networks, wavelength manipulation is essential for data routing, and optoelectronic shifters are employed to perform wavelength shifting; the optical signal is converted to an electrical signal and then back into an optical signal at a different wavelength. This creates an undesirable speed bottleneck. In order to overcome this problem, as well as to increase the bandwidth, all-optical networks have been proposed that would succeed their electrical counterparts. For these types of networks new types of optical devices are required that directly manipulate communication channels to shift their wavelength across the optical fiber bandwidth.

Non-linear processes in semiconductor devices have the potential to fill this technological gap where two wavelengths in a nonlinear material can be mixed to generate the sum or difference frequency, effectively shifting the original wavelengths.[3] Normally, however, these techniques are based on the small bulk non-linearities of the material, and demand phase matching for a long interaction length and/or high pump powers. These considerations can be overcome by using resonant non-linearities of quantum wells[6,7] which are orders of magnitudes greater than those of the bulk, permitting much shorter interaction lengths. Indeed considerable investigations have been undertaken of the wavelength shift of near infrared (NIR) beam in the presence of an intense THz beam in a quantum well system.[8-11] These studies were based on enhanced non-linear susceptibilities where the near-infrared beam was resonant with excitonic interband transitions and the THz beam was resonant with excitonic intersubband levels. The resonances could be modified to engineer the wavelength shift by changing the quantum well geometry[10] or by the application of an external electric field[12,13] and large efficiencies (0.1% - 0.2%) could be obtained.[14,15] However, an important point of all this work is that the THz beam is provided by an entire facility - the free electron laser (FEL) - and thus prohibiting its relevance to real world applications.

THz QCLs[4,16] are recently realised semiconductor sources that operate in the THz range. QCLs are based on intersubband transitions where laser action takes place between confined conduction band subbands in a series of coupled quantum wells. The intracavity fields (upto a few kV/cm) of these devices can approach those that are used in the FEL studies mentioned above.[15] QCLs therefore have the potential as an integrated wavelength converter to shift an external NIR beam by the QCL frequency by (i) providing large intracavity powers and (ii) an enhanced non-linearity from the interband resonance of the NIR beam with the confined states. Previous work using QCLs and a NIR beam took advantage of the bulk second order non-linearity of GaAs to perform frequency mixing[17] or the use of a double resonant process[18] but the efficiencies of the processes were limited ($10^{-4}$ -$10^{-3}$ %). Here, we demonstrate an improvement of 2 orders of magnitude with conversion efficiencies of up to 0.13 %, comparable to those obtained in FEL investigations.

Figure 1a shows the schematic of the process investigated here via the resonant interband excitation of the QCL with the NIR beam. The THz QCL laser transition $E_{QCL}$ occurs within the conduction band between the highlighted green states (green wave arrow). A NIR beam $E_{NIR}$ (red arrow) is coupled into the QCL cavity and resonantly tuned with an interband transition implying hole and electron states. As a result the difference frequency is generated $E_{NIR}$-$E_{QCL}$ (dark red arrow), via a virtual state and the THz photon (green arrow), which is below the bandgap and therefore avoids absorption.[10] (The reverse situation also occurs with an excitation at the virtual transition to generate the sum frequency, $E_{NIR}$+$E_{QCL}$, at the bandgap).

Figure 1b shows the geometry of the experiment where the input interband excitation and the THz QCL emission are collinear i.e. in the same plane parallel to the surface of the QCL. This is in strong contrast to previous experiments that have investigated resonant non-linear mixing where the THz beam and near-infrared excitation were orthogonal.[10,12,15,18] This type of guided geometry for both the THz beam and input interband excitation allows the use of a much longer interaction length. The NIR pump is coupled into one QCL facet and the difference frequency exits the opposite facet as well as the remaining input (the latter depending on the optical losses).

The guided modes are shown in Figure 1c for the THz QCL emission and the injected NIR beam (just below bandgap) using a dual wavelength waveguide. The confinement of the transverse magnetic (TM) polarised THz beam is based on a standard surface plasmon mode. The NIR excitation (transverse electric (TE) or TM) is confined by the top metal layer and a 300nm $Al_{0.5}Ga_{0.5}As$ grown between the lower doped layer and the substrate. This layer has a lower refractive index than the surrounding material and therefore dielectrically confines the injected NIR beam.

QCLs operating at 2.8THz using GaAs/AlGaAs quantum wells and based on a bound-to-continuum design[19] were employed and operated in continuous wave at 10K. (See method section for more details on the sample and experimental set-up). Figure 2a show the spectra of the beam without transmission through the QCL with the pump beam centred at $E_{NIR}$=1.5267eV ($\lambda$=812nm) i.e. just above the effective bandgap of the QCL and corresponding to electronic transitions between the first confined hole and electron states. The polarisation of the NIR beam was chosen to be parallel to that of the QCL (i.e. TM polarized) implying interband transitions from only the light hole states.[20] Figure 2b shows the spectrum after transmission through the QCL driven below laser threshold (black curve) where $E_{NIR}$ is just visible, as a result of a parasitic part of the beam that does not pass through the ridge. The situation changes drastically when the QCL is above threshold (red curve). The difference frequency is clearly observed at $E_d$=$E_{NIR}$-$E_{QCL}$= 1.5152eV (λ=818nm), i.e. separated from the pump $E_{NIR}$ by exactly the photon energy of the THz QCL (f=2.78THz) and is below the bandgap of the material. A point to note is the high apparent conversion efficiency, with the difference frequency 14 times more intense than the pump wavelength (taken as the ratio of the integrated signals of the pump and sideband). This is due to the sharp interband absorption. To estimate the actual conversion efficiency, defined as the ratio of the power of the sideband divided by that of the input NIR pump $P_d/P_{NIR}$, the coupling efficiency of the pump needs to be determined. This was done by characterising the transmission of the pump at an energy below the effective gap of the QCL where the interband losses are zero. This allows the determination of the NIR pump intensity coupled into the input facet of the QCL. With this calibration taken into account an efficiency of 0.13% is determined.

The inset of figure 3a shows the interest of this technique for THz detection. A high resolution spectrum of the sideband (with the pump at 1.528eV) showing many modes is shown which is an exact replica of the QCL Fabry Perot emission and which was taken in less than a second. This shows that this wavelength conversion allows one to measure and upconvert the THz emission of the QCL to the near-infrared. Further, these measurements used standard CCD camera technology for detection. The spectrum exhibits a 1.2 GHz resolution which is comparable to that of a considerably slower high resolution FTIR spectrometer.

The resonant nature of interaction can be seen in figure 3a where spectra for several pump wavelengths and their corresponding difference frequency for a TM pump polarisation are shown. For clarity, the curves have been normalised by setting the pump wavelength intensities to one. As the pump energy is increased from 1.522eV to 1.534eV the difference frequency increases in intensity showing a double resonance before decreasing at higher pump energies. These results are plotted in figure 3b and show the efficiency with the absorption of the pump taken into account (see above) as a function of the pump energy (square points). Resonances at 1.531eV and 1.527eV are observed with the latter showing a conversion efficiency of 0.13% which was the highest obtained. This is more than two orders of magnitude greater than previously demonstrated frequency mixing using QCLs. The full width at half maximum of each resonance is ~1 – 2 meV. These resonances arise when $E_{NIR}$ is resonant with interband transitions that have a large overlap between the electron and hole wavefunctions. Also shown in figure 3b is the efficiency with a TE polarised NIR beam corresponding to interband excitation predominately from heavy holes states.[20] One resonance is clearly observed at 1.525 eV and another broader one around 1.528 eV. The slightly lower energy of the resonance for the TE polarization compared to that of the TM is due to the higher confinement of the heavy hole states. The slighty reduced efficiency in the TE polarisation is due to the smaller overlap of the electron and heavy hole states.

To identify the states involved in the nonlinear process, the photoluminescence (PL) from the QCL was investigated (Figure 4b). As the PL emission is given by the transitions having the lowest energy, i.e. involving heavy holes states, it is compared to the efficiency curve for a TE polarization of the NIR pump (figure 4a, red squares). The TE efficiency is also plotted as a function of the difference energy $E_{NIR}$-$E_{QCL}$ (green circles). Firstly, regarding the resonances in the efficiency at the pump beam energies (red squares), the main peak corresponds to the shoulder in the PL spectrum at 1.525 eV and that the higher energy and broader resonance corresponds to a transition around 1.527 eV. Secondly, no peaks are seen in the PL in the difference energy range (green circles) illustrating that there are no resonant transitions and confirming that the wavelength conversion is realized through a virtual state below the bandgap. (The small shoulder at 1.519eV is due to PL from the GaAs substrate).

Figure 4c shows a comparison between the PL spectrum with the overlap of the interband wavefunctions of the QCL, the PL being proportional to the square of the overlap between the electron and hole states.[21,22] Figure 4d presents the bandstructure of the studied sample including conduction and valence bands. The states taken into account are highlighted and are the three lowest lying heavy hole levels (labelled H1 to H3) and five electronic states in the miniband (labelled E1 to E5) which have a significant overlap. Comparing figures 4a, 4b and 4c, the efficiency peak at 1.525eV is a result of resonances with HH1E1 and HH1E2 transitions i.e. the lowest lying states. The higher energy broader resonance is more difficult to identify to a sole transition and appears to be related multiple contributions between the three hole states and the lower electron states. This explains the broader nature of the second resonance. A similar analysis can be performed for the light hole states that shows only a significant overlap comes between the lowest lying hole state and the lowest electronic states that are separated by 3meV, in agreement with the results of figure 3b. Thus the nonlinear process is singly resonant with the lowest energy hole states and the electronic states of the QCL's miniband.

It is possible to estimate the second order susceptibility, $\chi^{(2)}$, from the efficiency, $\eta$:[23-25]

$$\eta = \frac{P_d}{P_{NIR}} = \frac{8\pi^2 \left|\chi^{(2)}\right|^2 L^2 P_{QCL}}{\varepsilon_0 n_{NIR} n_{QCL} n_d c \lambda_d^{\,2} S} e^{-\alpha_p \frac{L}{2}} \frac{\sin^2\left(\frac{\Delta k L}{2}\right) + sh^2\left[\alpha_p \frac{L}{4}\right]}{\left(\frac{\Delta k L}{2}\right)^2 + \left(\alpha_p \frac{L}{4}\right)^2} \qquad [1]$$

where $P_d$ ($n_d$), $P_{NIR}$ ($n_{NIR}$), $P_{QCL}$ ($n_{QCL}$) are the intensities (refractive indices (~ 3.6)) of the generated beam, the input NIR pump, and the THz QCL respectively, L is the cavity length of the QCL (1.5mm), $\lambda_d$ is the generated wavelength (818nm) and S is the interaction area defined as the modal overlap between the three interacting waves (8000 $\mu m^2$) [17]. The intracavity THz power is 75mW, estimated from the detected output power and a facet reflectivity of 0.32. $\alpha_p$ are the losses of the NIR pump (estimated at 1000 $cm^{-1}$)[20] and $\Delta k$ is the phase mismatch. Here the losses of the difference frequency and the THz beam are taken as zero. Although phase matching in the geometry presented here is possible due to refractive index dispersion at resonance[26] (see supplementary material S2), the high losses of the pump beam is the limiting factor regarding the interaction length. Equation 1 can then be simplified to:

$$\eta = \frac{P_d}{P_{NIR}} \approx \frac{64\pi^2 \left|\chi^{(2)}\right|^2 P_{QCL}}{\varepsilon_0 n_{NIR} n_{QCL} n_d c \lambda_d{}^2 S} \frac{1}{\alpha_p} \qquad [2]$$

Taking the maximum efficiency of 0.13 %, a second order non-linearity of $\sim 1\times10^4$ pm/V is determined. This is rough agreement with previous studies which have shown interband nonlinearities in the range of $10^2$-$10^4$ pm/V for quantum wells[27,28] confirming that the non-linear susceptibility is enhanced by the resonant excitation.[29]

We have shown that the resonant interband properties of a QCL can be used for efficient frequency mixing through enhanced nonlinearities. The perspectives on this work are wide ranging. The wavelength shift can be engineered to any desired THz value[30] and can be equally applied to MIR QCLs,[31] where the wavelength shift is much greater and can be used to shift between different telecommunication bands[32]. As well as room temperature and high power output,[33] MIR QCLs are based on InGaAs/AlInAs quantum wells where the interband transition is directly in the telecommunication range. Further increases in efficiencies could be realised through a) adapted active region designs or the insertion of passive quantum wells to enhance the non-linearity through optimisation of the overlaps between the confined states; and b) the combination of intersubband non-linearities with those of the interband transitions. This work also shows the potential to efficiently up convert the QCL emission permitting the use of NIR technology for the detection of THz emission or providing a NIR-THz link for free space telecommunications. On a more fundamental side, this work also opens up the possibility of studying high THz-optical field interactions using compact and powerful QCLs, previously reserved to entire facilities such as the FEL.

In conclusion an efficient wavelength converter based on a compact QCL was demonstrated. Frequency conversion with high efficiencies was realised through the enhancement of the non-linearity where the pump is resonant with interband transitions, combined with the high THz intra-cavity power density. These developments show the potential of QCLs as novel optical components for the all-optical telecommunication networks.

## Methods

QCLs operating at 2.8THz using GaAs/AlGaAs quantum wells and based on a bound-to-continuum design were employed (12μm active region thickness). Samples were processed into a single plasmon geometry with a ridge width of 250μm and a cavity length of 1.5mm. The samples were operated in continuous wave at 10K. (See supplementary material S1 for the optical and electrical characteristics as well as the spectrum). As the bandgap of GaAs is in the near-infrared, the interband pump was sourced from a CW Ti:Sapphire laser that also allowed a large wavelength tunability and permits the correct interband resonance excitation to be found. 100 μW of NIR pump power was used with a coupling efficiency of ~20%, resulting in ~20μW coupled into the QCL cavity. Low powers for the input NIR beam were used so as not to affect the QCL performance. This was verified by confirming that the threshold current observed in the change in differential resistance of the VI did not increase with the coupled NIR beam. The transmitted NIR beam is collected at the opposite facet using a high numerical aperture objective and analysed using a spectrometer coupled to a thermoelectrically cooled CCD camera.

## References


1. Eldada, L. Optical communication components. *Rev. Sci. Instrum.* **75**, 575-593 (2004).

2. Desurvire, E. Capacity demand and Technology Challenges for Lightwave Systems in the Next Two Decades. *J. Lightwave Technol.* **24**, 4697-4710 (2006).

3. Campi, D. & Coriasso, C. Wavelength conversion technologies. *Photon. Network Commun.* **2**, 85–95 (2000).

4. Köhler, R. *et al.* Terahertz semiconductor-heterostructure laser. *Nature* **417**, 156-159 (2002).

5. DeCusatis, C., Maass, E., Clement, D.P. & Lasky, R.C. Eds. *Handbook of Fiber Optic data Communication* (Academic Press, 1998).

6. Sirtori, C., Capasso, F., Faist, J., Pfeiffer, L.N. & West K.W. Far-infrared generation of doubly resonant difference frequency mixing in a coupled quantum well two dimensional electron gas system. *Appl. Phys. Lett.* **65**, 445-447 (1994).

7. Belkin, M.A., Terahertz quantum-cascade-laser source based on intracavity difference-frequency generation. *Nature Photonics* **1**, 288-292 (2007).

8. Kono, J. *et al.* Resonant Terahertz Optical Sideband Generation from Confined Magnetoexcitons. *Phys. Rev. Lett.* **79**, 1758-1761 (1997).

9. Černe, J. Near-infrared sideband generation induced by intense far-infrared radiation in GaAs quantum wells. *Appl. Phys. Lett.* **70**, 3543-3545 (1997).

10. Phillips, C., Su, M.Y., Sherwin, M.S., Ko, J. & Coldren, L. Generation of first-order terahertz optical sidebands in asymmetric coupled quantum wells. *Appl. Phys. Lett*. **75**, 2728-2730 (1999).

11. Carter, S.G. *et al.* Terahertz-optical mixing in undoped and doped GaAs quantum wells: From excitonic to electronic intersubband transitions. *Phys. Rev. B.* **72**, 155309 (2005).

12. Ciulin, V., Carter, S.G., Sherwin, M.S., Huntington, A. & Coldren, L.A. Terahertz optical mixing in biased GaAs single quantum wells. *Phys. Rev. B.* **70**, 115312 (2004).

13. Su, M.Y., Carter, S.G., Sherwin, M.S., Huntington, A. & Coldren, L.A. Voltage-controlled wavelength conversion by terahertz electro-optic modulation in double quantum wells. *Appl. Phys. Lett.* **81**, 1564-1566 (2002).

14. Wagner, M. *et al.* Resonant enhancement of second order sideband generation for intraexcitonic transitions in GaAs/AlGaAs multiple quantum wells. *Appl. Phys. Lett.* **94**, 241105 (2009).

15. Carter, S.G. *et al*. Terahertz electro-optic wavelength conversion in GaAs quantum wells: Improved efficiency and room-temperature operation. *Appl. Phys. Lett.*, **84**, 840-842 (2004).

16. Williams, B.S., Terahertz quantum cascade lasers. *Nature Photonics* **1**, 517-525 (2007).

17. Dhillon, S.S. *et al.* Terahertz transfer onto a telecom optical carrier. *Nature Photon.* **1**, 411-415 (2007).

18. Zervos, C. *et al.* Coherent near-infrared wavelength conversion in semiconductor quantum cascade lasers. *Appl. Phys. Lett.*, **89**, 183507 (2006).

19. Barbieri, S. *et al.* 2.9 THz quantum cascade lasers operating up to 70 K in continuous wave. *Appl. Phys. Lett.*, **85**, 1674-1676 (2004).

20. Rosencher, E. & Vinter B. *Optoelectronics* 2nd ed. (Dunod, 2002).

21. Freeman, J.R., Brewer, A., Beere, H.E. & Ritchie, D.A. Photo-luminescence study of heterogeneous terahertz quantum cascade lasers. *J. Appl. Phys.* **110**, 013103 (2011).

22. Vitiello, M. S. *et al.* Measurement of subband electronic temperatures and population inversion in THz quantum cascade lasers. *Appl. Phys. Lett.* **86**, 111115 (2005).

23. Sutherland, R.L., McLean, D. G. & Kirkpatrick, S. *Handbook of nonlinear optics* (CRC Press, 2003).

24. Rosencher, E. & Bois, Ph. Model system for optical non-linearities; Asymmetric quantum wells. *Phys. Rev. B.* **44**, 11315 (1991).

25. Yariv, A. *Quantum Electronics* 3rd ed. (Wiley, 1989).

26. Blakemore, J.S. Semiconducting and other major properties of gallium arsenide, *J. Appl. Phys.* **53**, R123-R181 (1982).

27. Garmire, E., Kost, A. & Khurgin, J. *Nonlinear optics in semiconductors II* (Academic Press, 1999).

28. Khurgin, J. Second-order nonlinear effects in asymmetric quantum-well structures. *Phys. Rev. B.* **38**, 4056 (1988).

29. This rather large range in simulated and experimental nonlinearities is a result of interband nonlinearities being a complex problem that involves the contribution of many real and virtual band-to-band transitions.[28]

30. Scalari, G. THz and sub-THz quantum cascade lasers. *Laser & Photon. Rev.* **3**, 45–66 (2009).

31. Faist, J. Quantum Cascade Laser. *Science* **264**, 553-556 (1994).

32. Shin, W., Han S.W., Park, C.S. & Oh, K. All fiber optical inter-band router for broadband wavelength division multiplexing. *Opt. Express.* **12**, 1815-1822 (2004).

33. Lu, Q.Y., Bai, Y., Bandyopadhyay, N., Slivken, S., & Razeghi, M. 2.4 W room temperature continuous wave operation of distributed feedback quantum cascade lasers. *Appl. Phys. Lett.* **98**, 181106 (2011).

**Acknowledgements**

This work was financially supported by the "Programme Francilien de Recherche en Nanosciences" (CNano-IDF, contract TeraConversion) and the "Agence Nationale de la Recherche" (ANR, contract "HI-TEQ" ANR-09-NANO-017). The author J.R.F would like to acknowledge funding from the Marie Curie Action fellowship (Grant no. 274602). The author J.M. would like to acknowledge funding from French Ministry of Defense (DGA). The "Laboratoire Pierre Aigrain" (LPA) is a "Unité Mixte de Recherche Associée à l'ENS, au Centre National de la Recherche Scientifique (CNRS) UMR8551 et aux Universités Paris 6 et 7". The device fabrication was performed at the nanocenter "La Centrale de Technologie Universitaire" (CTU-IEF-Minerve), which was partially funded by the "Conseil General de l'Essonne".

**Author contributions** J.M. and P.C. set up the experiment acquired the experimental data and contributed equally. S.S.D conceived the experimental concept. PL measurements were taken by J.R.F, K.M. and P.C. Sample growth was performed by H.E.B and D.A.R. The manuscript was written and the data interpreted by J.M, P.C, J.R.F, N.J., J.M., J.T, C.S and S.S.D. C.S. gave insight and interpretation of the nonlinear properties of QCLs. All work was coordinated and overseen by J.T. and S.S.D.

**Materials and correspondence** should be addressed to sukhdeep.dhillon@lpa.ens.fr

**Competing Interests statement** The authors declare that they have competing financial interests (patent application filed).

## Figure Captions

**Figure 1| Scheme principle and optical modes**. **a,** Schematic of the resonant non-linear process for the generation of the difference frequency ($E_{NIR}$-$E_{QCL}$) in a QCL operating at $E_{QCL}$ (green wave arrow between states $E_u$ and $E_n$). A NIR pump $E_{NIR}$ (red arrow) is tuned in resonance with interband transitions involving hole states in the valence band and electron states in the miniband of a QCL. This allows the generation of a lower energy beam (dark red arrow) at $E_{NIR}$-$E_{QCL}$ via a virtual state below the material bandgap (dotted line) and the THz photon (green arrow). (For clarity the process is shown for one quantum well). **b,** Schema of the geometry and the experimental principle. A NIR beam, $E_{NIR}$, is coupled into the cavity of a QCL operating at $E_{QCL}$ via one facet (left side of the figure). The transmitted $E_{NIR}$ and the difference frequency $E_{NIR}$-$E_{QCL}$ are collected through the opposite facet. **c,** Intensity profiles of the THz QCL mode at 2.8THz (green line) and the NIR mode (red line) of the dual wavelength QCL waveguide. The NIR mode is confined between the metallic upper contact layer and an AlGaAs layer insuring a maximum overlap with the active region of the QCL.

**Figure 2| Wavelength shifting using interband excitation. a,** Spectrum of the NIR pump, $E_{NIR}$, before coupling into the QCL cavity. **b,** Spectrum of the transmitted beam with QCL below laser threshold (black curve). Spectrum of the transmitted beam with QCL above laser threshold (red curve). A high intensity peak appears at $E_{NIR}$-$E_{QCL}$ i.e $E_{NIR}$ shifted by the energy of the QCL frequency (2.78 THz).

**Figure 3| Resonant behavior and polarization effect of NIR pump. a,** Spectra of the QCL output for different pump excitation energies. The pump beams are normalized to 1. $E_g$

corresponds to the energy from which the NIR pump is absorbed, showing that the generated beam is always below the absorption edge. Insert: High resolution spectrum of the generated beam that corresponds to the QCL emission intensity spectral profile. **b,** Conversion efficiency as a function of the NIR pump energy with losses taken into account for TE polarization (red dots) and TM polarization (black squares) of the input pump beam. The solid curves are gaussian fits to the data.

**Figure 4| Confined states involved in resonant nonlinear interaction. a,** Conversion efficiency for TE polarization of the NIR pump as a function of the generated difference beam energy (green dots) and the pump energy (red squares). **b,** Photoluminescence spectrum of the QCL biased above laser threshold (i.e. for wavelength shifting). **c,** Overlaps of the interband transitions involving the 3 lowest lying heavy holes states (HH1, HH2 and HH3) and the electronic states of the lower miniband of the QCL (states E1 to E5). **d,** Bandstructure of the QCL showing the valence (heavy holes) and conduction band states. The states in bold lines are those with significant overlap in the range of energies where the difference frequency is observed. The calculated overlaps in (c) correspond to transitions between HH1 (black), HH2 (magneta) and HH3 (blue) with miniband states increasing in energy from E1 through to E5. The QCL laser transition is represented by a green wave arrow between the upper and lower laser states.

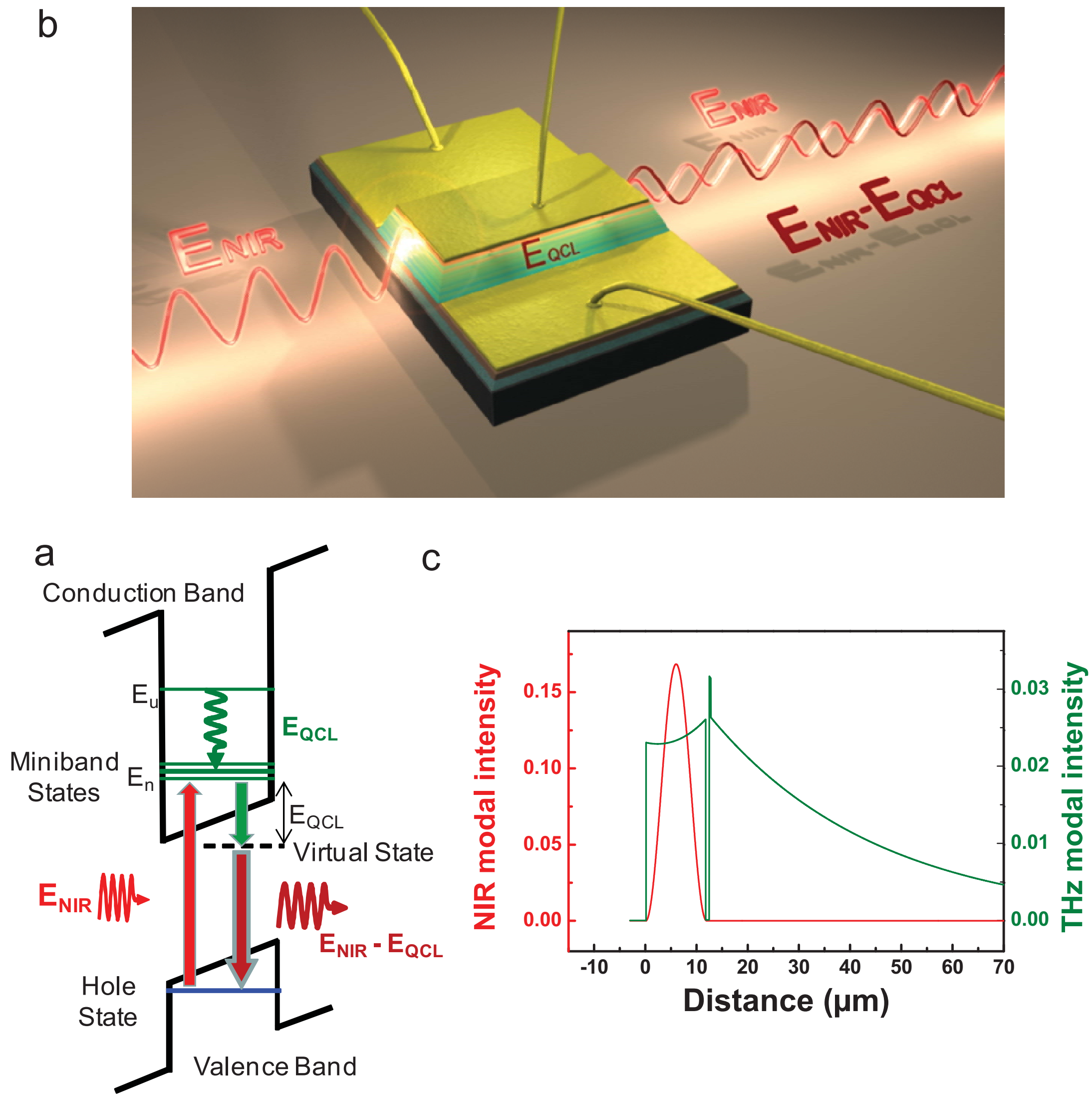
b
E_NIR
E_QCL
E_NIR-E_QCL
a
Conduction Band
E_u
E_QCL
Miniband States
E_n
E_QCL
Virtual State
E_NIR
E_NIR - E_QCL
Hole State
Valence Band
c
NIR modal intensity
THz modal intensity
0.00
0.05
0.10
0.15
0.00
0.01
0.02
0.03
-10 0 10 20 30 40 50 60 70
Distance (μm)

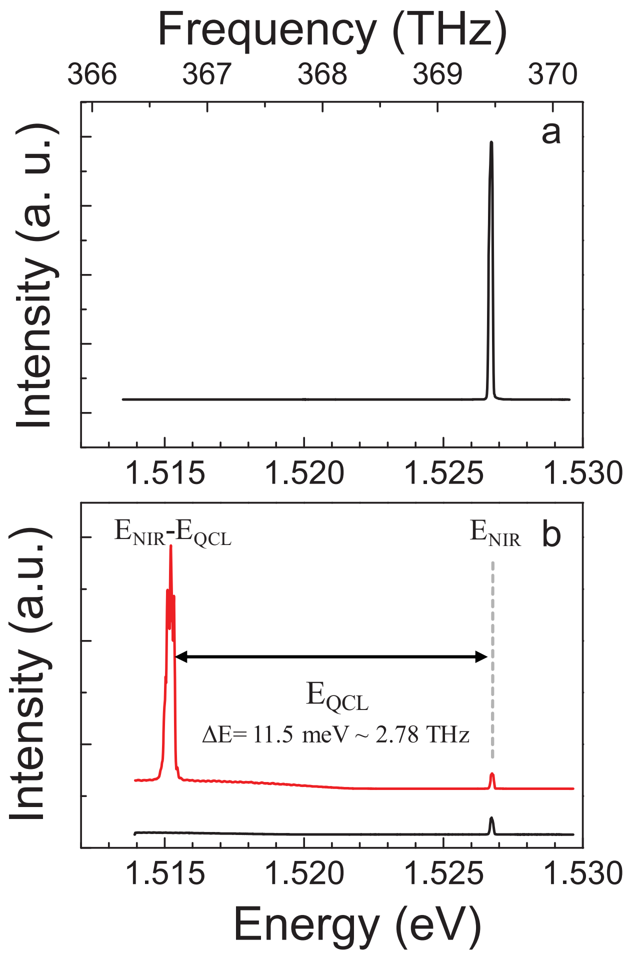

Frequency (THz)
366
367
368
369
370
a
Intensity (a. u.)
1.515
1.520
1.525
1.530
E_NIR-E_QCL
E_NIR
b
E_QCL
ΔE= 11.5 meV ~ 2.78 THz
Intensity (a.u.)
1.515
1.520
1.525
1.530
Energy (eV)

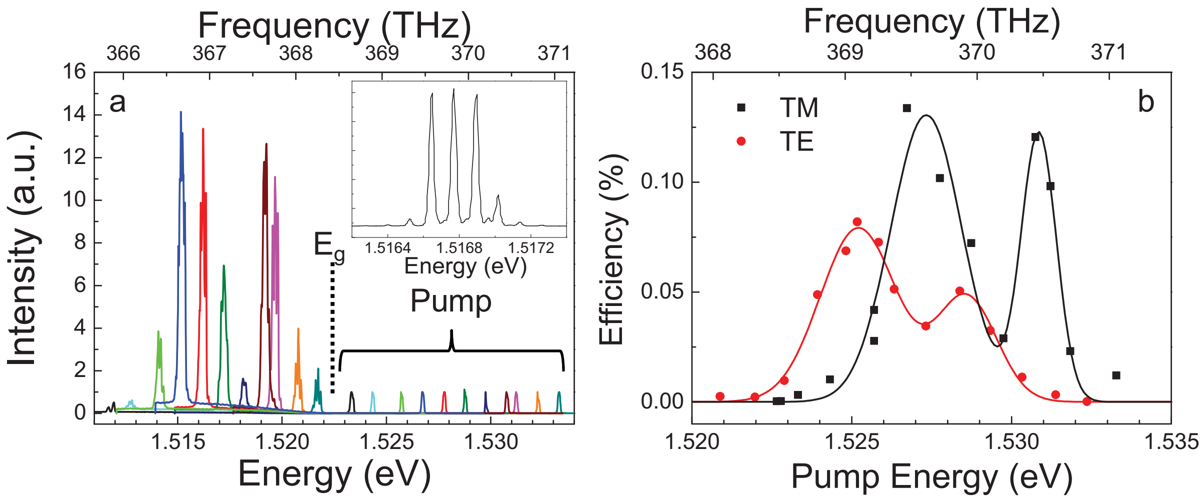

Frequency (THz)
366
367
368
369
370
371
16
14
12
10
8
6
4
2
0
a
Intensity (a.u.)
1.515
1.520
1.525
1.530
Energy (eV)
$E_g$
Pump
1.5164
1.5168
1.5172
Energy (eV)
Frequency (THz)
368
369
370
371
0.15
0.10
0.05
0.00
Efficiency (%)
TM
TE
b
1.520
1.525
1.530
1.535
Pump Energy (eV)

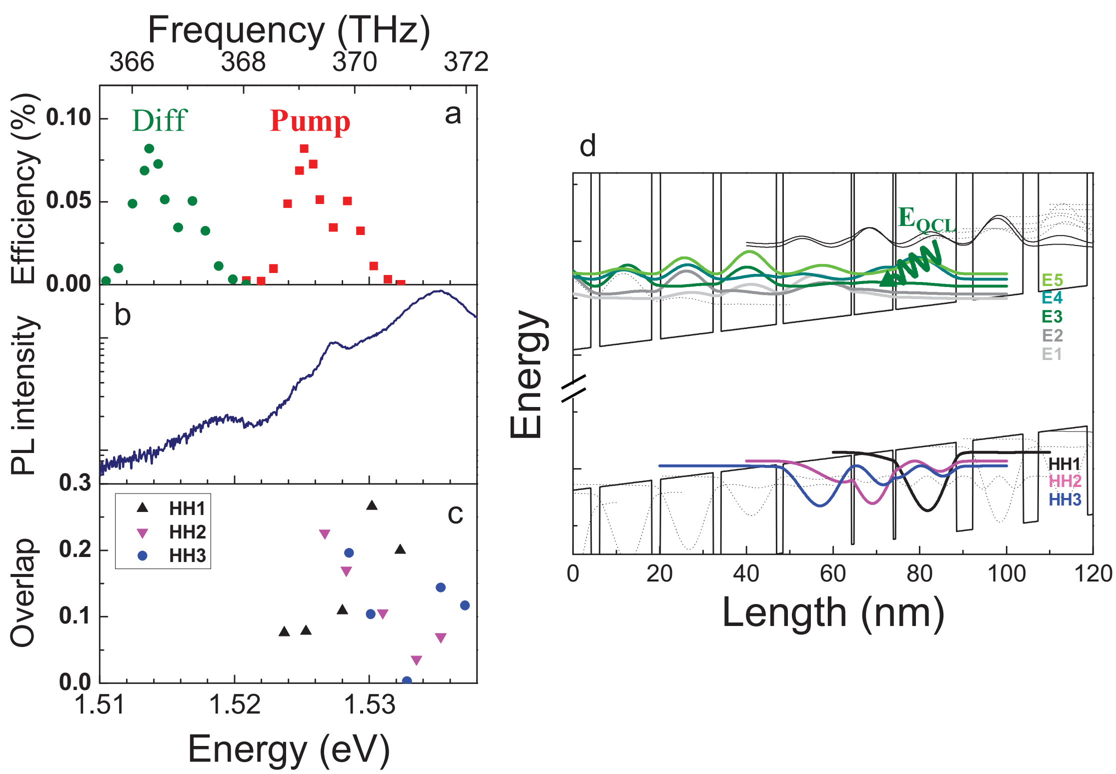

Frequency (THz)
366
368
370
372
Diff
Pump
a
Efficiency (%)
0.10
0.05
0.00
b
PL intensity
0.3
c
HH1
HH2
HH3
Overlap
0.2
0.1
0.0
1.51
1.52
1.53
Energy (eV)
d
$E_{QCL}$
E5
E4
E3
E2
E1
Energy
HH1
HH2
HH3
0
20
40
60
80
100
120
Length (nm)